Interdecadal Modulation of the Impact of ENSO on Precipitation and Temperature over the United States

KINGTSE C. MO

NOAA/NWS/NCEP/Climate Prediction Center, Camp Springs, Maryland

(Manuscript received 7 December 2009, in final form 23 February 2010)

ABSTRACT

Data from observations and the Intergovernmental Panel on Climate Change (IPCC) twentieth-century climate change model [phase 3 of the Coupled Model Intercomparison Project (CMIP3)] simulations were analyzed to examine the decadal changes of the impact of ENSO on air temperature T_{air} and precipitation P over the United States. The comparison of composites for the early period (1915–60) and the recent period (1962–2006) indicates that cooling (warming) over the south and warming (cooling) over the north during ENSO warm (cold) winters have been weakening. The ENSO influence on winter P over the Southwest is strengthening, while the impact on P over the Ohio Valley is weakening for the recent decades. These differences are not due to the long-term trends in T_{air} or P; they are attributed to the occurrence of the central Pacific (CPAC) ENSO events in the recent years. The CPAC ENSO differs from the canonical eastern Pacific (EPAC) ENSO. The EPAC ENSO has a sea surface temperature anomaly (SSTA) maximum in the eastern Pacific. Enhanced convection extends from the date line to the eastern Pacific, with negative anomalies in the western Pacific. The atmospheric responses resemble a tropical Northern Hemisphere pattern. The wave train is consistent with the north–south T_{air} contrast over North America during the EPAC ENSO winters. The CPAC ENSO has enhanced convection in the central Pacific. The atmospheric responses show a Pacific–North American pattern. It is consistent with west–east contrast in T_{air} and more rainfall over the Southwest during the CPAC ENSO winters.

1. Introduction

El Niño–Southern Oscillation (ENSO) has large impact on precipitation P and air temperature T_{air} over the United States (Ropelewski and Halpert 1986, 1989). Recently, many studies have suggested that the impact of ENSO is not stationary. For example, van Oldenborgh and Burgers (2005) documented that the strength of teleconnections between ENSO and P varied with time during the last century. Kumar et al. (1999) observed that the relationship between ENSO and the Indian monsoon has been weakening. Over the United States, correlations between ENSO and P anomalies over the western region were higher during the recent periods in comparison to the early period from 1920 to 1950 (McCabe and Dettinger 1999). Diaz et al. (2001) found that correlations between ENSO and P over the Southeast were higher after the 1980s. While these studies are informative, observational studies are often limited by the data availability. Physical mechanisms associated with these decadal changes are not fully understood.

The common method to quantify the impact of ENSO is to form composites. The average of P or T_{air} over ENSO years during the study period is considered as the mean impact of ENSO for that period. The assumption is that all ENSO events have similar characteristics and impacts within random fluctuations. If there are two or more types of ENSO events and they have different impacts, then the above assumption is no longer valid. One needs to address the impact of ENSO for each type separately.

Many studies suggested that there are two types of ENSO events (Ashok et al. 2007; Yeh et al. 2009). Larkin and Harrison (2005a,b) found that the type of ENSO that has a sea surface temperature anomaly (SSTA) maximum in the central Pacific (CPAC ENSO) near the date line has a different impact on P and T_{air} from the convectional ENSO with an SSTA maximum in the eastern Pacific (EPAC ENSO). Recently, Kao and Yu (2009)

Corresponding author address: Kingtse Mo, 5200 Auth Rd., NOAA/NWS/NCEP/Climate Prediction Center, Camp Springs, MD 20746.
E-mail: kingtse.mo@noaa.gov

DOI: 10.1175/2010JCLI3553.1

and Kug et al. (2009) examined these two ENSO events in detail. The EPAC ENSO is associated with the basin-scale processes along the equator. Large SSTAs are located over the Niño-3 region. The evolution of the EPAC ENSO is similar to the ENSO composites of Rasmusson and Carpenter (1982). It has the mean duration of 15 months. The CPAC ENSO has large SSTAs in the Niño-4 region and is also labeled as the warm pool ENSO (Kug et al. 2009). The CPAC ENSO is related to local processes. The zonal advection plays an important role in the evolution. The CPAC ENSO is often associated with anomalous westerlies over the western and central Pacific and anomalous easterlies over the eastern Pacific. It also has shorter duration of only 8 months. Ashok et al. (2007) examined two EOF patterns of SSTAs in the tropics. The first EOF is associated with the EPAC ENSO. The second pattern with warming in the central Pacific and cooling east of 120°W resembles the CPAC ENSO. They labeled that type of ENSO as Modoki ENSO. The EPAC ENSO is more common. The CPAC events started to appear after 1960 (Yeh et al. 2009). Because two ENSO types have different convection patterns and atmospheric responses, it is expected that they will have different impacts on the hydroclimate over the United States.

The major problem associated with observational studies of the CPAC ENSO is the limited sample size. Composites may depend on the events that are selected or the data that are used. The observed datasets are not long enough to have robust statistics for diagnostic studies. One possibility is to rely on many ocean–atmosphere coupled GCM experiments to confirm the observational findings. The Intergovernmental Panel on Climate Change (IPCC) twentieth-century climate change model—phase 3 of the Coupled Model Intercomparison Project (CMIP3)—simulations (Meehl et al. 2007) are well suited for this purpose. The drawback of the model experiments is that all of the models have errors. If the ensemble means are able to capture the impact of both types of ENSO, then they can be used as a diagnostic tool to study physical mechanisms.

The goals of this paper are 1) to relate the decadal changes of the ENSO impact on P and T_{air} over the United States to the CPAC and EPAC events; and 2) to use IPCC twentieth-century climate change model simulation (20C3M) experiments to examine the physical mechanisms associated with the ENSO impacts. Datasets used and procedures of analyses are described in section 2. The decadal changes of the ENSO impact over the United States based on composites are documented in section 3. These changes are linked to the occurrence of the CPAC ENSO and EPAC ENSO in section 4. Because there were only seven CPAC ENSO events, the IPCC 20C3M runs were used to study the physical mechanisms associated with two types of ENSO. Conclusions are given in section 5.

2. Data and procedures

a. Observations

The study period is from 1915 to 2006. The monthly mean P and T_{air} data were obtained from the University of Washington. The gridded datasets are based on the cooperative station meteorological daily data (Andreadis et al. 2005). The P data were corrected with the Precipitation Regression on Independent Slopes Method (PRISM). The resolution is 0.5°. These were the same forcing data used by Andreadis et al. (2005) to study drought. The SST data are the monthly reconstructed SSTs from Smith et al. (1996). The Extended Reconstructed SST version 2 (ERSST v2) is used, and the horizontal resolution is 2°. The sea level pressure (SLP) for the Northern Hemisphere is available from 1899 to the present from the National Center for Atmospheric Research (NCAR) Web site (Trenberth and Paolino 1980). Climatological monthly means for the study period were removed from each dataset to obtain anomalies.

The composites were calculated separately for the early period (1915–60) and the recent period (1962–2006). Because the influence of ENSO is seasonally dependent, composites for warm and cold events were computed separately for each season and each period. For each season, there are at least seven events in the composite. To document the evolution of the changes, composites were also performed for four 40-yr periods separated by 15 yr: 1915–55, 1930–70, 1945–85, and 1960–2000. There are at least five or more events in each composite.

The criteria used to select ENSO events for model simulations and observation are the same. The index used to select ENSO events is the normalized seasonal mean Niño-3.4 index (5°S–5°N, 170°E–120°W). Harrison and Larkin (2005a,b) used the monthly mean Niño-3.4 index to classify ENSO events. A warm (cold) ENSO event was identified when the Niño-3.4 index was greater than 0.5° (less than −0.5°) for three consecutive months. The model simulations have errors. The magnitudes of the Niño-3.4 index simulated by models vary a great deal. Therefore, the normalized Niño-3.4 index was used. A warm (cold) ENSO event was selected when the index was above 0.8° (or below −0.8°) for that season. Reasonable variations of the criteria will not change the conclusions. There were, on average, 5 (10) warm (cold) events per season for the early period (1915–55). The number of warm (cold) events increased (decreased) with time. There were, on average, 11 (6) warm (cold) events for the recent period (1960–2006). There were more warm events in the recent period. To the first order of approximation, the patterns of warm and cold ENSO composites are similar, but with an opposite sign. To increase the sample size, results are presented as the weighted differences between warm and cold events as

$$\text{diff} = \frac{\text{compo(warm)} \times \text{num(warm)} - \text{compo(cold)} \times \text{num(cold)}}{\text{num(warm)} + \text{num(cold)}}, \quad (1)$$

where compo(warm) is the composite map for warm events and num(warm) is the number of warm events in the composite. Cold cases are defined the same way.

The statistical significance of a composite is determined by the Monte Carlo method. Composites were formed based on randomly selected maps from the same P or T_{air} anomaly time series. The process was repeated 500 times. The statistical significance of the tested map can be determined from these 500 cases at each grid point. The composite should be within five percentiles of the distribution function determined by the composites of randomly selected maps. The areas in which values of the composite field are statistically significant at the 5% level are colored.

b. *IPCC models*

For the model study, the focus is on winter [January–March (JFM)] warm ENSO events because the impact of ENSO over the United States is strong. The 20C3M IPCC experiments are studied. The model outputs are available from the Program for Climate Model Diagnosis and Intercomparison (PCMDI; online at http://www.pcmdi.llnl.gov/ipcc). The detailed documentation of 20C3M can also be found there.

Van Oldenborgh et al. (2005) evaluated the ENSO cycle simulated by the CMIP models. They compared the simulated ENSO patterns and the time series of ENSO variability in the tropical Pacific with observations. They also examined the strength of the coupled atmosphere–ocean feedback mechanisms of ENSO (Bjerknes 1966; Wyrtki 1975) in the model simulations. Based on the evaluation, they found five models as that simulate realistic ENSO. These five models are Geophysical Fluid Dynamics Laboratory Climate Model version 2.1 (GFDL CM2.1), GFDL Climate Model version 2.0 (GFDL CM2.0), Model for Interdisciplinary Research on Climate 3.2, medium-resolution version [MIROC3.2(medres)], the third climate configuration of the Met Office Unified Model (HadCM3), and Max Planck Institute (MPI) ECHAM5. These are models analyzed here.

For a given model, there are many members in the ensemble. The model resolution and total simulated years are given in Table 1. For each member and each variable, winter monthly mean anomalies were obtained by removing the winter mean climatology from that member. All members are treated equally. The EPAC and CPAC events were selected from each member based on Niño-3 (5°S–5°N, 90°–150°W) and Niño-4 (5°S–5°N, 160°E–150°W) indices. The total number of ENSO events for a given model is the sum of events from all members in the ensemble. If the Niño-3 index is greater than 0.8 standard deviations, and it is also greater than the Niño-4 index by a predetermined number delta, then the event is classified as an EPAC event. If the Niño-4 index is greater than 0.8 standard deviations, and is also greater than the Niño-3 index by delta, then it is classified as a CPAC event. Delta is assumed to be 0.3°C for all models except MIROC3.2(medres), which has very weak SSTAs in the tropics so that delta is 0.1°C. If the criteria vary slightly, then there will be either more or less events, but the results will not change. The purpose here is not to count the number of events but to select events from the model runs that mimic the observed SSTA patterns. Events were selected for each model. The number of events for each model is given in Table 1. Together, there are 104 total EPAC events and only 51 total CPAC events. The ratio is approximately 2:1, consistent with results reported by Yeh et al. (2009). For each model, composites for the CPAC and EPAC events were computed for SSTA, SLP, P, and T_{air} from the pooled time series of winter mean anomalies. The statistical significance is based on the Student's t test, and each event is considered as one degree of freedom. Because models have different resolutions, all of the model outputs were interpolated to 2.5° resolution before averaging. The ensemble mean is the equally weighted average of all models.

3. Decadal variations of the impact of ENSO based on observations

In this section, the decadal changes of the impact of ENSO on P and T_{air} over the United States are examined by composites. Then, these changes are related to the occurrence of the EPAC and CPAC events.

a. *Composites for early and recent periods*

Discussions in this section are based on warm events. The situation reverses for cold events. Composites of

TABLE 1. CGCM from the IPCC twentieth-century model experiments analyzed in this study.

Model	Resolution lat × lon	Total years	CPAC events	EPAC events
GFDL CM2.1	90 × 144	700	17	34
GFDL CM2.0	90 × 144	420	8	7
MIROC3.2(medres)	64 × 128	453	12	13
MPI ECHAM5	96 × 192	814	10	23
HadCM3	73 × 96	280	4	27

seasonal mean T_{air} are displayed for the early (1915–60) and recent (1961–2006) periods in Fig. 1, while the evolution of changes is given in Fig. 2. The strong responses in T_{air} occur in winter. Both periods show cooling over the south and Southeast and warming over the north and Northwest, consistent with Ropelewski and Halpert (1986, 1989), but the magnitudes of anomalies and details differ. For the early period, winter composite shows cooling over the areas south of 40°N and east of 105°W, including the Southeast, the southern Plains, and the Gulf States and warming over the areas north of 42°N (Fig. 1a). The cooling over the south and Southeast reached a peak during 1930–70, with negative anomalies extending from Texas to the East Coast and from the Gulf of Mexico to 38°N (Fig. 2b). After that, the influence has been weakening. The composite for the recent period shows weak anomalies confined to the areas south of 34°N and the Atlantic Coast (Fig. 1e). For spring [April–June (AMJ)], the composite shows warming over the areas roughly west of 110°W, including the Pacific Northwest and the western interior states for the early period (Fig. 1b). For the areas west of 100°W and north of 36°N, the strongest warming occurred in spring during the period of 1915–55 (Fig. 2e). After that, warming was confined to the Pacific Northwest and cooling occurred in the southern Plains after the 1960s. The ENSO influence is weak during summer [July–September (JAS)]. For autumn [October–December (OND)], cooling has been shifting eastward.

For the early period, the influence of ENSO on P during winter (Fig. 3a) indicates wetness over northern California and the Southeast and dryness over the Pacific Northwest north of 42°N and the Ohio Valley centered at 38°N, 95°W. For the recent period, the influence of ENSO over California, Arizona, and Louisiana has been strengthening while the impact over the Ohio Valley has been weakening. The influence over the Great Plains has been weakening for AMJ and OND. The negative anomalies over the Pacific Northwest occurred early in OND instead of JFM (Figs. 3d,h). The impact in JAS is small. Similar to T_{air}, these changes started around 1960s.

The changes of the ENSO impact are related to the changes of SSTA and circulation anomalies. For the early period, the SSTA composite resembles an EPAC ENSO with a maximum located near 120°W (Fig. 4a). The composite of SLP anomalies shows a wave train with negative anomalies over the West Coast, positive anomalies over the eastern Canada, and negative anomalies extending from the Southeast to the Atlantic (Fig. 4c). For the recent period, the SSTA composite shows that the maximum of the SSTAs shifts to near 150°–160°W, which suggests possible contributions from the CPAC ENSO events. The SLP anomaly composite indicates a shifted response to SSTAs. The Aleutian low shifted southeastward in the recent decades. In the Atlantic, negative anomalies shifted eastward and weakened, and positive anomalies shifted northeastward. Many model experiments indicate that the atmospheric responses to ENSO depend on the location and magnitudes of SSTAs (Hoerling and Kumar 2002; Hoerling et al. 1997). The changing hydroclimate over the United States during ENSO is consistent with the atmospheric responses to the changing SSTA patterns.

There are few possible reasons for such changes. There were more warm events and less cold events in the recent decades. The differences in climatology between two periods could make differences. For example, there were warming trends in the March–May minimum temperature (Groisman et al. 2004) over the western region during the past 60 yr. For precipitation, there were the two driest periods in the 1930s and the 1950s followed by the increase of rainfall over the western mountains and the Great Plains (Mo and Schemm 2008). To examine this possibility, composites were computed with and without the mean for the period removed. They are similar so the differences are not due to the climatological differences in P or T_{air}.

The second possibility is that the behavior of ENSO is changing. The changes in the mean climate may modulate the teleconnections. That may trigger different responses to ENSO. The third possibility is that there are two types of ENSO. They have different impacts on the hydroclimate over the United States. Composites with all ENSO events together are the weighted means of two types of ENSO.

b. Influence of the CPAC and EPAC ENSO

In this section, we will investigate these two possibilities. Composites of P, T_{air}, SSTA, and SLP anomalies were performed for CPAC ENSO and EPAC ENSO events for the recent period (1961–2006). There was no CPAC before 1960, so only the EPAC ENSO events contributed to the composites for the early period. If the ENSO impact changes with time, then composites of the EPAC ENSO

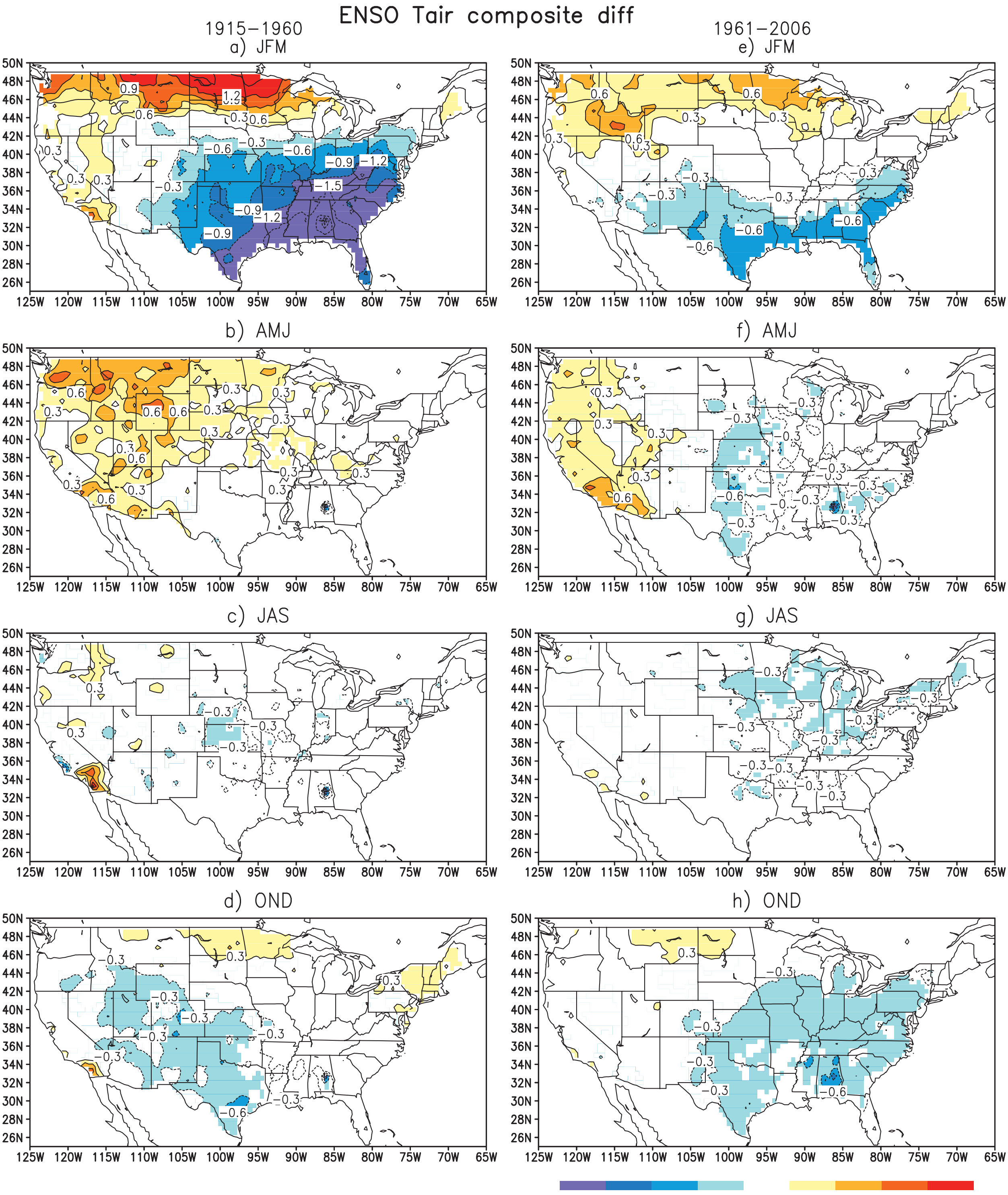

FIG. 1. Weighted composite difference of T_{air} anomalies between warm and cold ENSO events for (a) JFM, (b) AMJ, (c) JAS, and (d) OND for the early period (1915–60). Contour interval is 0.3°C. Zero contours are omitted. Areas where differences are statistically significant at 5% level based on the Monte Carlo test are colored. (e)–(h) As in (a)–(d), but for the recent period (1961–2006).

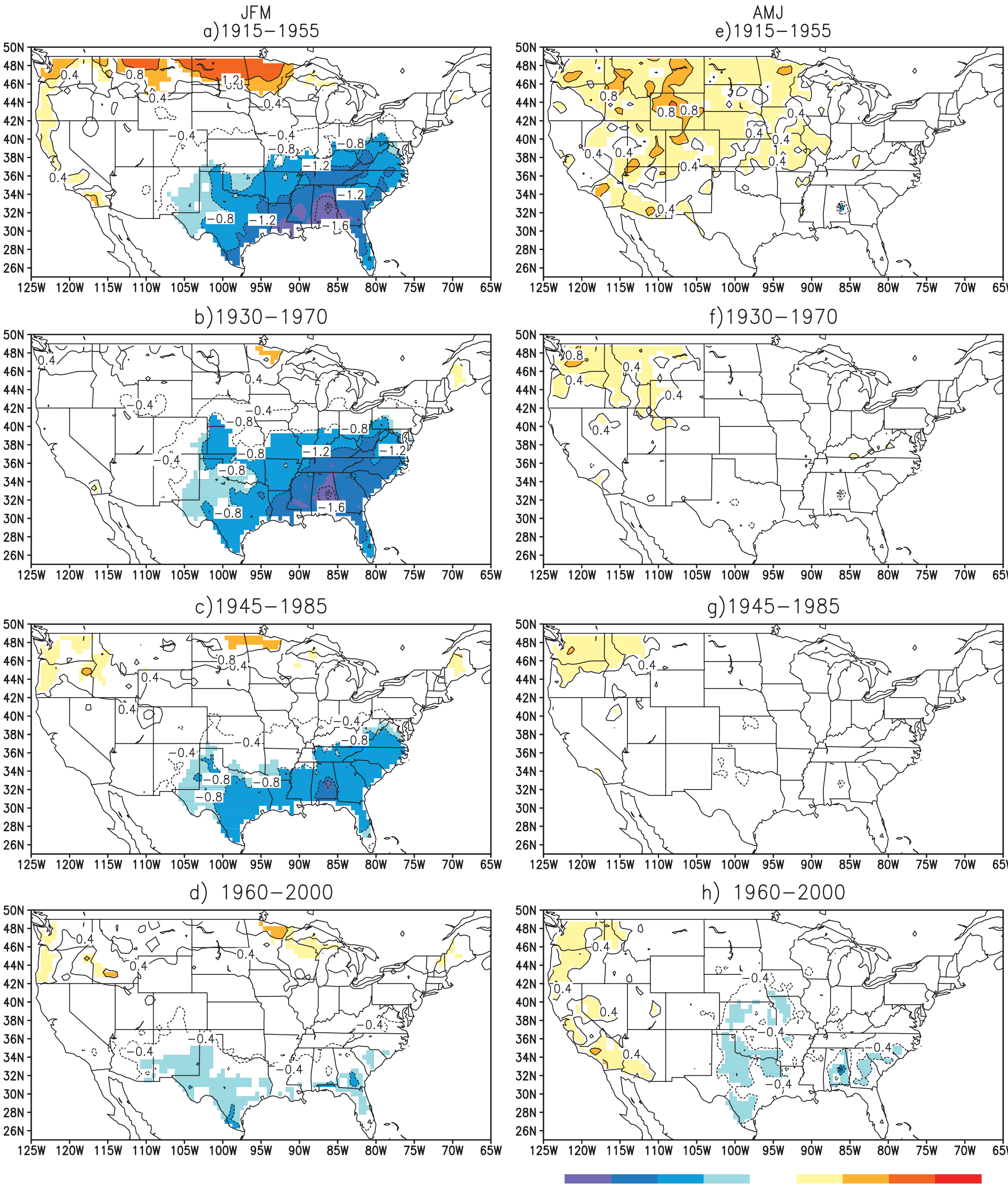

FIG. 2. Weighted composite difference of T_{air} anomalies between warm and cold ENSO events for JFM for the period (a) 1915–55, (b) 1930–70, (c) 1945–85, (d) 1960–2000. Contour interval is 0.4°C. Zero contours are omitted. Areas where differences are statistically significant at 5% level based on the Monte Carlo test are colored. (e)–(h) As in (a)–(d), but for AMJ.

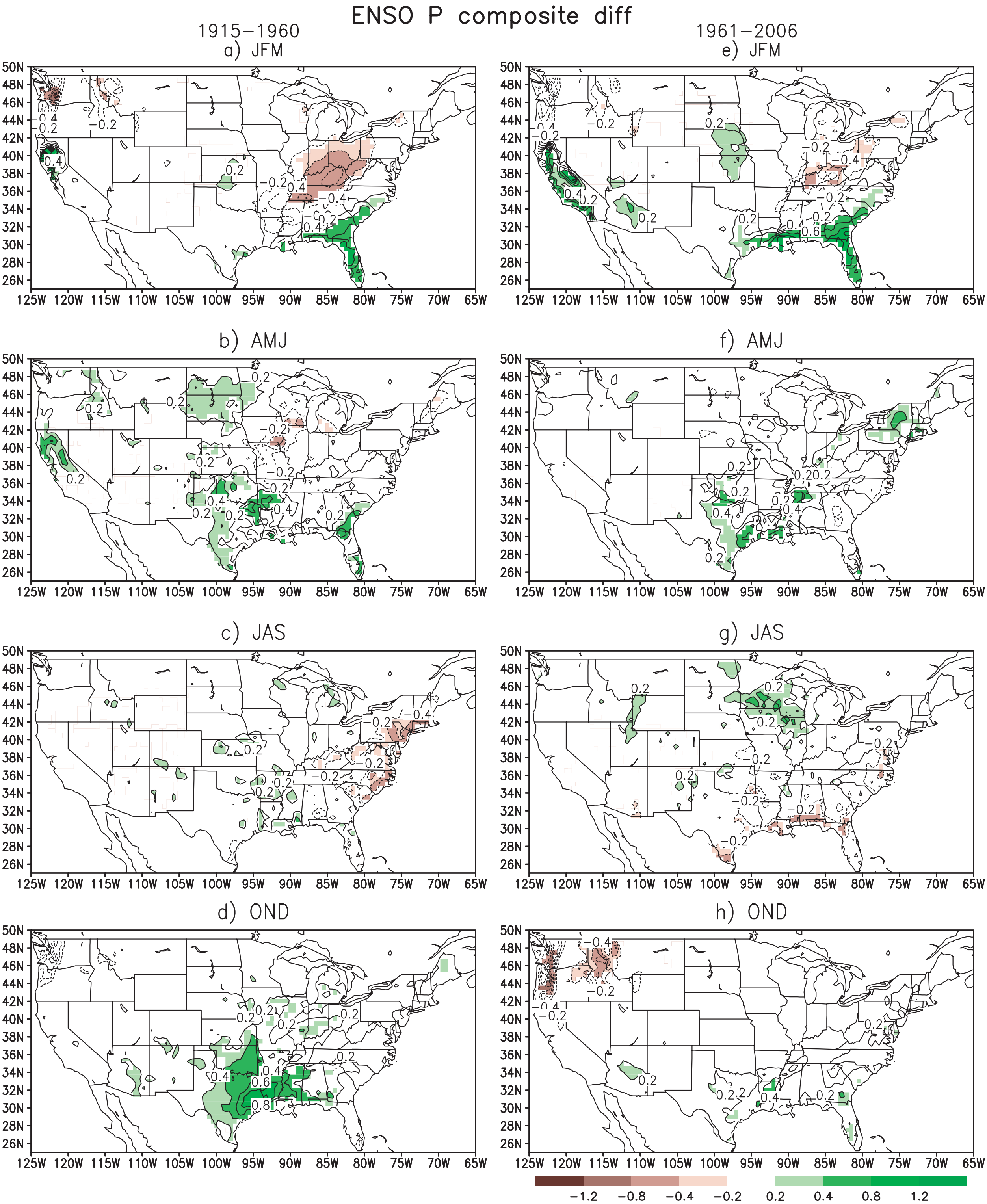

FIG. 3. Weighted composite difference of P anomalies between warm and cold ENSO events for (a) JFM, (b) AMJ, (c) JAS, and (d) OND for the early period (1915–60). Contour interval is 0.2 m day^{-1}. Zero contours are omitted. Areas where differences are statistically significant at 5% level based on the Monte Carlo test are colored. (e)–(h) As in (a)–(d), but for the recent period (1961–2006).

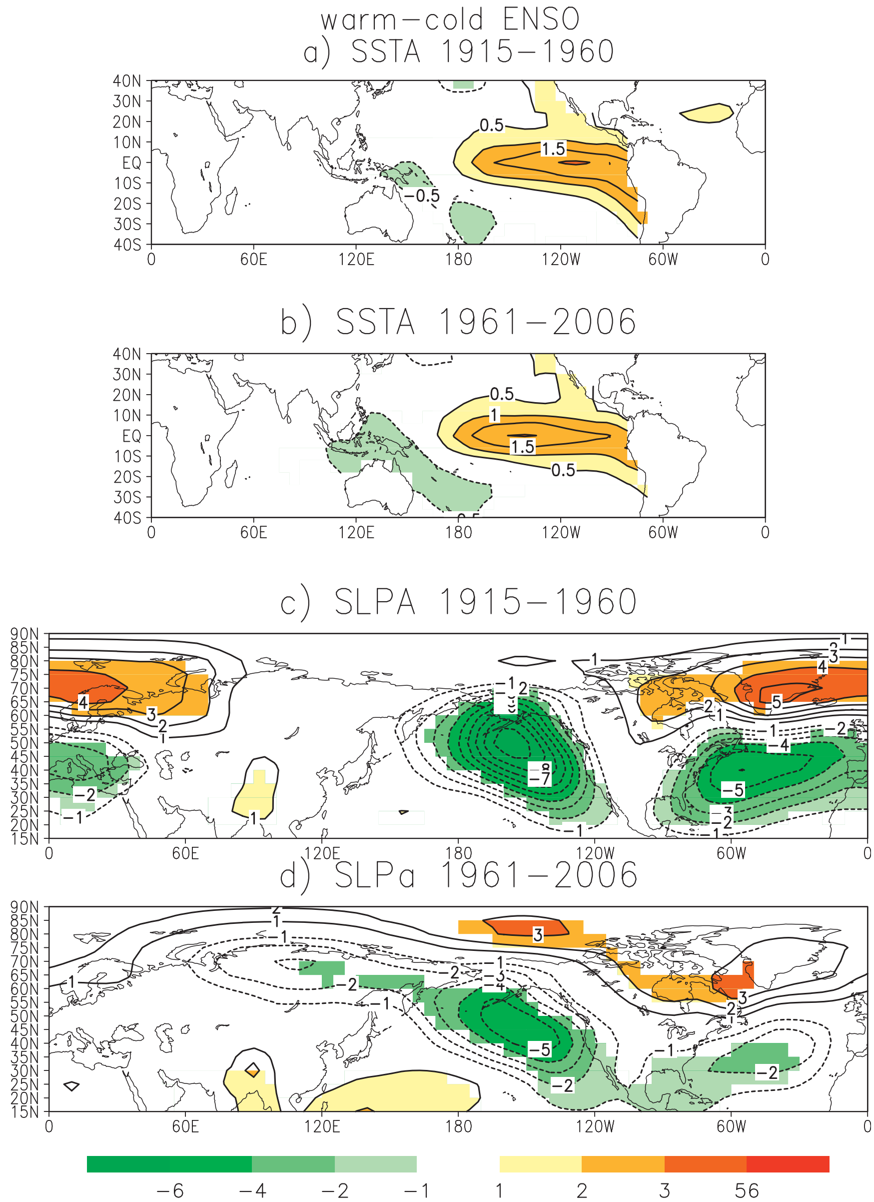

FIG. 4. Composite difference of SSTAs between warm and cold ENSO events for JFM for (a) the early period (1915–1960) and (b) the recent period (1961–2006). Contour interval is 0.5°C. Zero contours are omitted. Areas where differences are statistically significant at 5% level based on the Monte Carlo test are colored. (c) As in (a), but for SLP anomalies. Contour interval is 1 mb. (d) As in (c), but for the recent period.

for the recent period will differ from the composites for the early period. To test whether the decadal changes are due to the occurrence of the CPAC ENSO, linear combinations of the CPAC and EPAC ENSO composites are weighted by their numbers were compared with the composites for the recent period (Figs. 1 and 3).

The ENSO events were taken from the supplemental Table 1 from Yeh et al. (2009). Composites events from the detrended and raw SSTAs are similar. Figures 5 and 6 show composites from the events chosen from the detrended SSTs. The CPAC events entering the composites are in 1969, 1978, 1991, 1995, 2002, 2003, and 2005. The EPAC events are in 1964, 1966, 1970, 1973, 1977, 1980, 1983, 1987, 1988, 1991, 1998, and 2004.

The SSTA composite for the EPAC ENSO (Fig. 5a) shows a conventional SSTA pattern with warm SSTAs extending from 170°W to the eastern Pacific with a maximum near 120°W. The composite (Fig. 5a) is similar to the SSTA composite for the early period (Fig. 4a). The CPAC ENSO shows warm SSTAs extending from 170°W to the coast of California. There are no significant SSTAs in the eastern Pacific east of 120°W. Composites are similar to two types of ENSO discussed by Kug et al. (2009).

To examine whether the linear combinations of the CPAC and EPAC ENSO weighted by their numbers were able to explain the composites for the recent period, we computed the linear combination using the following formula:

$$\mathrm{comb} = \frac{\mathrm{compo(CPAC)} \times \mathrm{num(CPAC)} + \mathrm{compo(EPAC)} \times \mathrm{num(EPAC)}}{\mathrm{num(CPAC)} + \mathrm{num(EPAC)}}, \tag{2}$$

where compo(CPAC) is the composite of all CPAC events in the recent period and num(CPAC) is number of the CPAC ENSO events. Compo(EPAC) and num(EPAC) are defined the same way. The linear combination of SSTAs (Fig. 5c) is similar to the SSTA composite for the recent period (Fig. 4b). The SSTA maximum is located in the central Pacific.

The T_{air} composite of the CPAC ENSO events shows a west–east contrast of T_{air} anomalies with warming over the West and cooling over the Southeast and the Gulf States (Fig. 6d). Composites for the EPAC are similar to the composites for the early period (Figs. 1a and 6e). Both show a north–south contrast, with warming over the north and cooling over the south (Fig. 6e). The linear combination of the CPAC and EPAC ENSO (Fig. 6f) is similar to the composite for the recent period. It still shows a north–south contrast, but magnitudes of anomalies are weaker than the composite for the EPAC ENSO alone.

For P, the EPAC ENSO composite shows positive anomalies over northern California and the Southeast, and negative anomalies over the Pacific Northwest and the Ohio Valley. It is similar to the P composite for the early period (Fig. 3a). The CPAC ENSO shows stronger positive anomalies over the Southwest and weaker anomalies over the Southeast. The negative anomalies shift from the Ohio Valley southward to the Gulf States. Again, the linear combination of the CPAC and EPAC ENSO composites weighted by the number of events bears resemblance to the P composites for the recent period (Fig. 3e). The composites for SLP do not pass the statistical significant test so they will not be presented.

There are two types of ENSO and they have different impacts on the hydroclimate over the United States. The impact of the EPAC ENSO does not change with time. Composites for the recent period are similar to the linear combination of the CPAC and EPAC events. The differences of the impact of ENSO between the early and recent periods can be in part attributed to the more frequent appearance of the CPAC events. This also suggests that composites formed by pooling all ENSO events together are misleading. They are not physically meaningful. The impact of ENSO should be analyzed for two types of ENSO separately.

The drawback of the above analyses is that the sample size is too small. There were only seven CPAC events. Composites presented here differ from composites from Larkin and Harrison (2005a) because of different datasets, and a different criterion was used to select events. This suggests that the composites have large uncertainties. To address uncertainties and understand the physical mechanisms associated with two types of ENSO, we turn to the IPCC experiments. If there are two types of ENSO in the model simulations and they have similar influence of P and T_{air} over the United States, then the model runs can be used to examine the physical mechanisms associated with the impact.

4. IPCC model composites

a. Model simulations

Figure 7 shows composites of the SSTAs for the CPAC and EPAC events. The composites vary from one model to another, but all models show that the CPAC ENSO has a maximum in the central Pacific near 180°, and the EPAC ENSO has a maximum in the eastern Pacific near 120°E. This suggests that the criteria used to select events are reasonable. GFDL CM2.1, HadCM3, and MPI ECHAM5 have robust and realistic SSTAs. The MIROC3.2(medres) has very weak SSTAs in the tropics. It also has problems capturing the atmospheric responses to ENSO.

The ensemble means (Fig. 8) are able to capture the SSTA patterns for two types of ENSO events. They are similar to the composites of observations (Fig. 5), and the magnitudes are slightly stronger (Figs. 8a,d). The ensemble mean composite of T_{air} for the EPAC events shows the north–south contrast (Fig. 8b) similar to the observed pattern (Fig. 6e), but there are large uncertainties over the north-central United States resulting from large spread among models. All of the models (Fig. 9) are able to capture warming over eastern Canada and cooling over the southern Plains, Southeast, and the Gulf States.

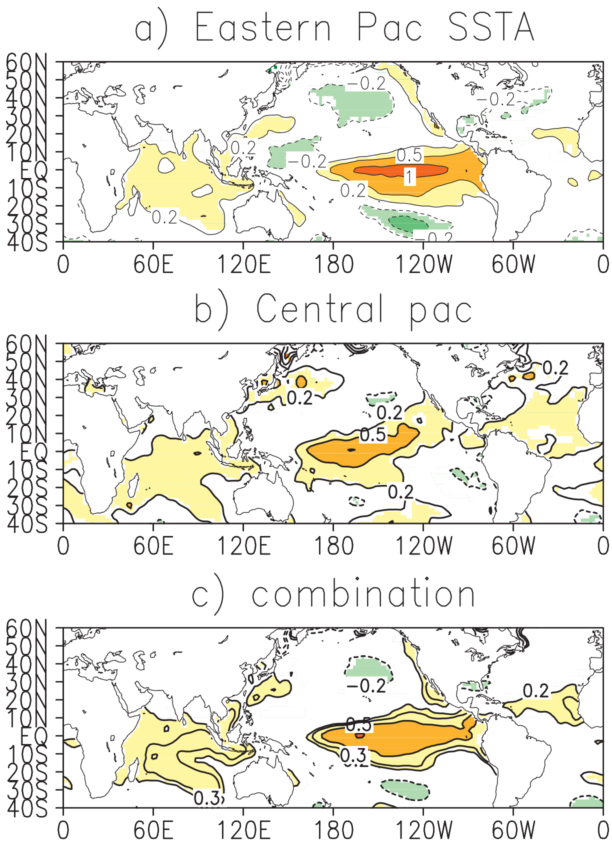

FIG. 5. (a) Composite of SSTAs of warm EPAC Pacific ENSO. Contour interval is 0.5°C. Contours −0.2° and 0.2°C are added. Zero contours are omitted. Areas where differences are statistically significant at 5% level based on the Monte Carlo test are colored. (b) As in (a), but for the CPAC ENSO events. (c) Weighted composite of the EPAC and CPAC events for the recent period.

Except for HadCM3, all of the models also show warming over western Canada and the Pacific Northwest. However, the zero line that separates warm from cold T_{air} anomalies varies from one model to another. Therefore, the statistically significant positive anomalies from the model shift northward in comparison with the observations (Fig. 6e). For the CPAC events (Fig. 8e), the ensemble mean shows the east–west contrast with cooling over the southern Plains and warming over the western states extends farther south, including over California. Both GFDL CM2.1 (Fig. 9f) and MPI ECHAM5 capture the east–west contrast while GFDL CM2.0 and MIROC3.2(medres) only show positive anomalies over the west. The composite from the HadCM3 is not realistic (Fig. 9j).

The ensemble mean P composites for the CPAC ENSO show more rainfall over the Southwest and less rainfall over the Southeast and the East Coast than the EPAC ENSO (Figs. 8c,f). While the ensemble responses are similar to the observations, the P composites from individual models are more diverse than T_{air} (Fig. 10). The EPAC ensemble mean captures the negative response over the Ohio Valley, but the CPAC ensemble mean does not capture the southward shift of anomalies from the Ohio Valley (Fig. 6a). The responses for MIROC3.2(medres) and MPI ECHAM5 do not pass the field significance test. Again, the GFDL CM2.1 has the most robust response and it is close to the observations.

The IPCC models show a lot of diversity. The combination of the observations and the ensemble means lets us to draw the following conclusions:

- There are two types of ENSO and they have very different impacts on P and T_{air} over the United States. The decadal changes of the ENSO impact can be attributed to the occurrence of the CPAC ENSO events.
- For T_{air}, the impact of the EPAC ENSO shows a north–south contrast, with warming over the north and cooling over the south, but the location of the zero line has large spread and uncertainty. The impact of the CPAC ENSO shows a west–east contrast, with warming over the West and cooling over the eastern United States. Cooling over the southern Plains and the Southeast is not as strong as the EPAC events. It is uncertain whether warming over the western region extends to the interior mountain region where data coverage is sparse.
- For P, the winter responses are the strongest. The CPAC events show more rainfall over the Southwest and less rainfall over the Southeast in comparison to the EPAC events. The response over the Ohio Valley has large uncertainty.

b. *Physical mechanisms*

GFDL CM2.1 is the most realistic model and the ENSO responses are close to the observations, so that outputs from that model were used to study the physical mechanisms associated with the impacts from both ENSO types. The GFDL CM2.1 simulation has 700 yr, and there are 34 EPAC events and 17 CPAC events.

The P composites (colored) in the tropics represent the convection associated with ENSO (Fig. 11). The conventional EPAC ENSO shows positive P anomalies extending from the central Pacific to the eastern Pacific and suppressed convection in the western Pacific. Negative P anomalies are also located to the south and north of positive anomalies in the Pacific because of the downward branches of the Hadley circulation. Negative P anomalies over northern Brazil are due to the Walker circulation as shown by the divergent wind anomalies (vectors). The rainfall over northeastern Brazil and over the Southeast is linked by local Hadley circulation. Suppressed convection in Brazil suggests favorable conditions for more rainfall over the Southeast.

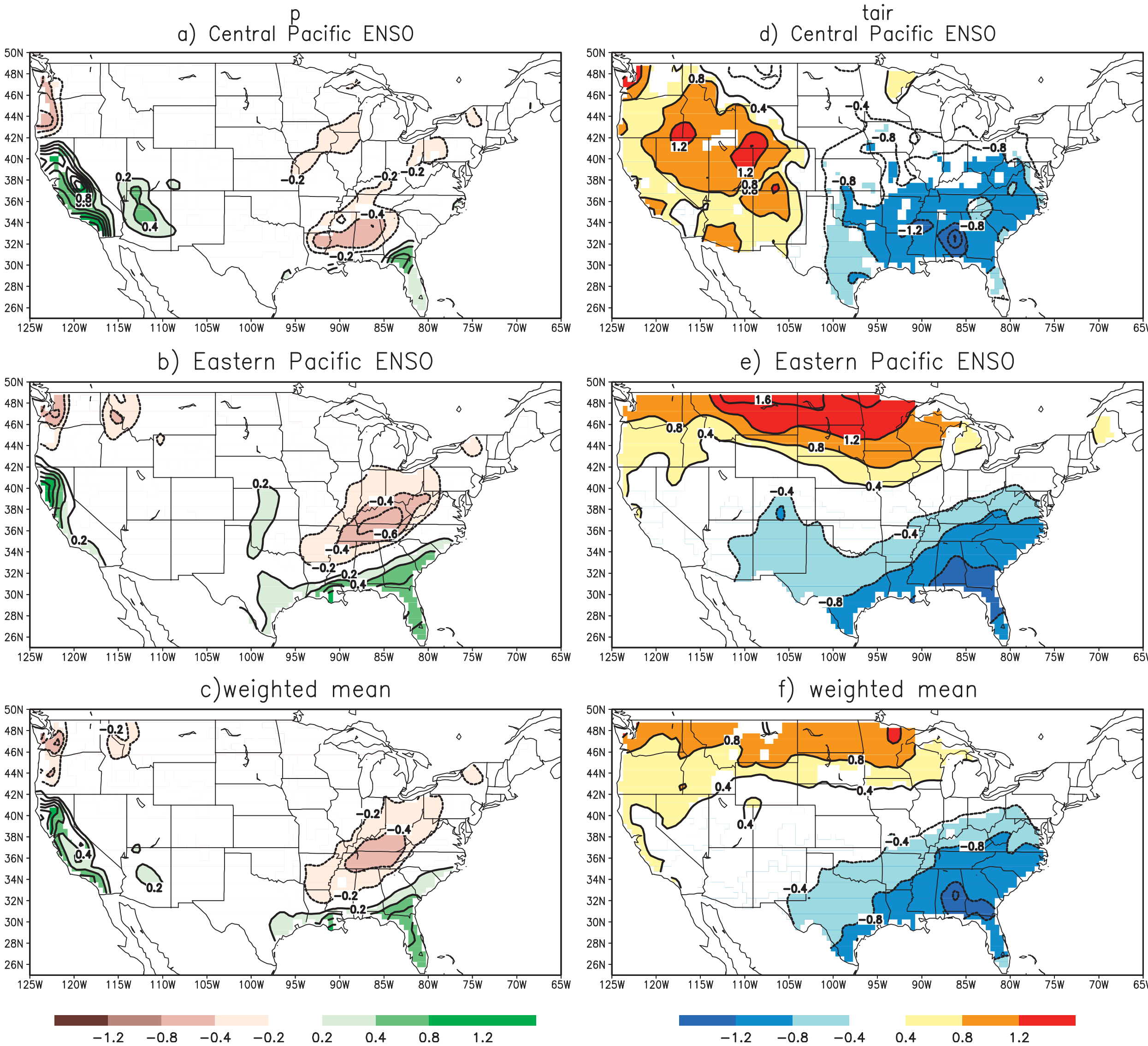

FIG. 6. (a) Composite of P for warm CPAC events for JFM. Contour interval is 0.2 m day^{-1}. Zero contours are omitted. Areas where differences are statistically significant at 5% level based on the Monte Carlo test are colored. (b) As in (a), but for EPAC ENSO. (c) As in (a), but for the weighted combination of the EPAC and CPAC events for the recent period. (d)–(f) As in (a)–(c), but for T_{air}. Contour interval is 0.4°C.

The streamfunction anomaly composite shows that a couplet straddles the equator over the convective area (Fig. 12a); this is a typical response to ENSO (Rasmusson and Mo 1993). Over North America, The response resembles a tropical Northern Hemisphere (TNH) teleconnection pattern, with positive anomalies over North America and negative anomalies to the west and east of the positive anomalies. This is consistent with warming over the north and cooling over the south. The zero line, which separates positive and negative T_{air} anomalies, depends on the exact locations and strength of the TNH wave train. It may vary from one event to another. Therefore, it has large uncertainty. The jet stream (colored) shows the extension of the subtropical jet to the east, and the North American jet shifts southward.

The situation for the CPAC events is different. For the CPAC events, convection is confined in the central Pacific near the date line (Fig. 11b). There is still suppressed convection over northern Brazil resulting from the Walker circulation, but the magnitudes of P anomalies are weaker. There is no cross-equatorial flow. The streamfunction composite shows a couplet along the equator, but it is located west of the EPAC couplet. The response in the

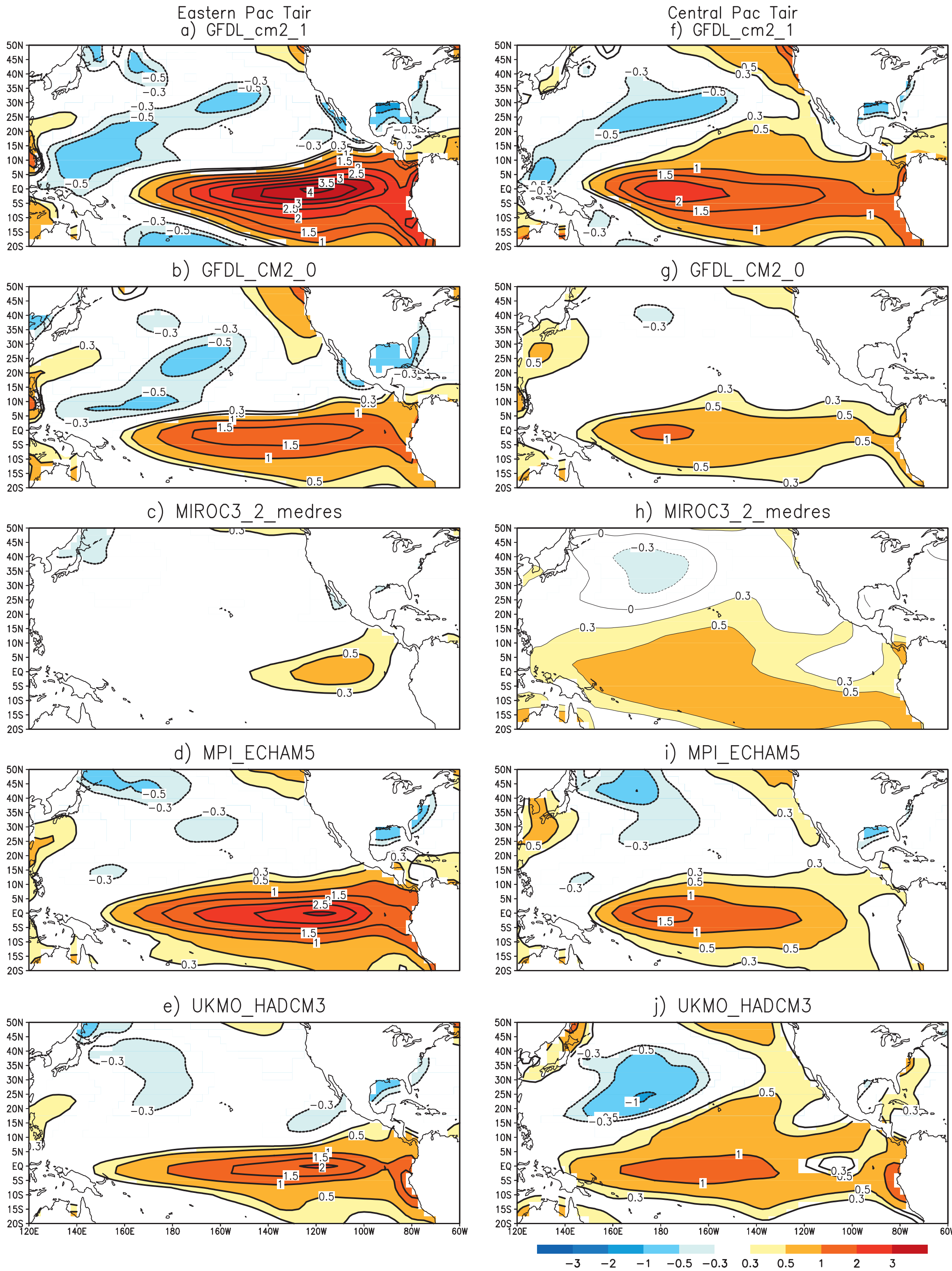

FIG. 7. Composite of SSTAs for EPAC ENSO events in (a) GFDL CM2.1, (b) GFDL CM2.0, (c) MIROC3.2(medres), (d) MPI ECHAM5, and (e) HadCM3. Contour interval is 0.5°C. Zero contours are omitted. Contours −0.3° and 0.3°C are added. Areas where differences are statistically significant at 5% level based on the Student's *t* test with one event as 1 degree of freedom are colored. (f)–(j) As in (a)–(e), but for CPAC ENSO.

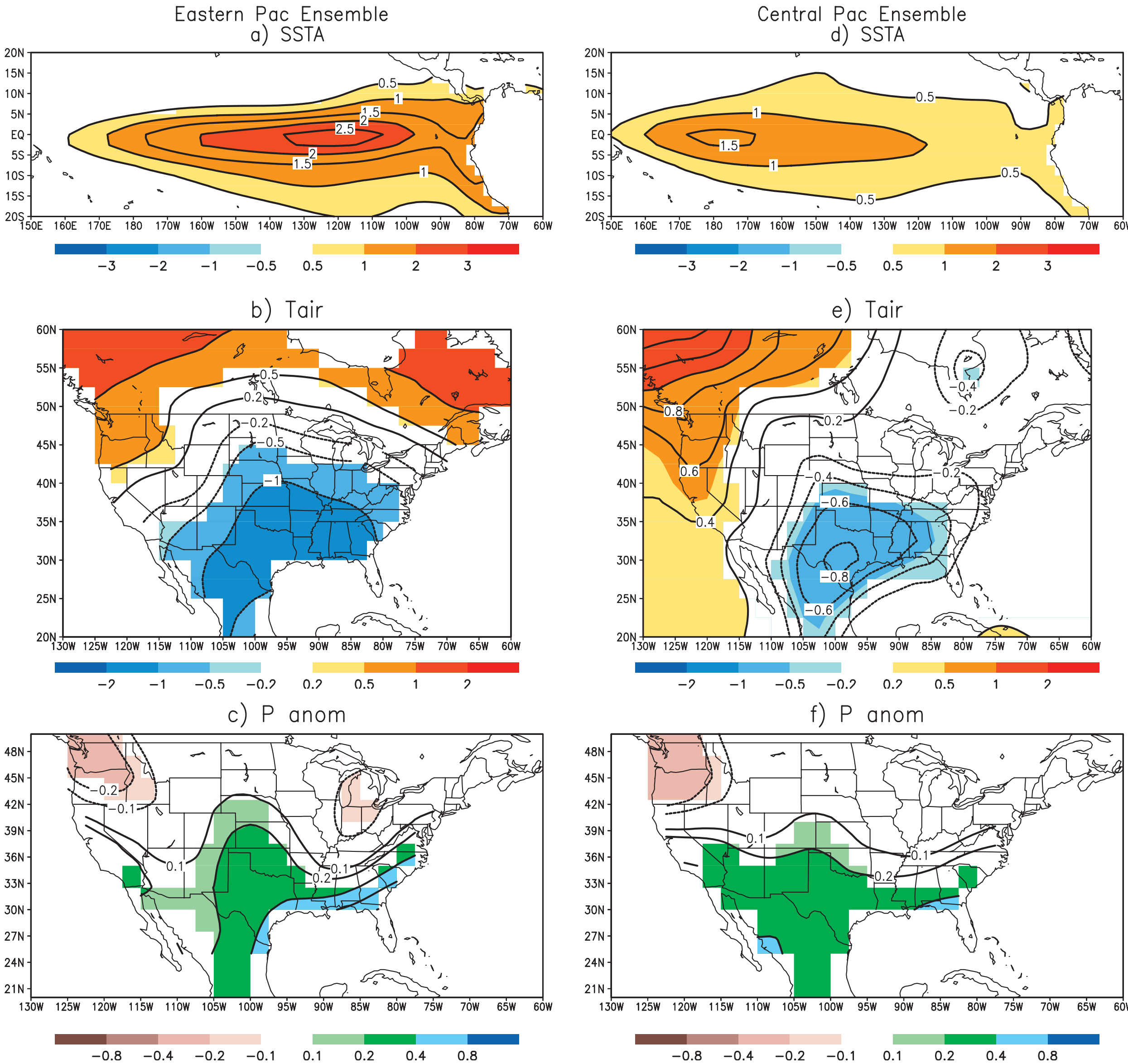

FIG. 8. (a) Composite of the SSTA ensemble mean for the EPAC ENSO. Contour interval is 0.5°C. Zero contours are omitted. Areas where values are statistically significant at the 5% level are colored. (b) As in (a), but for T_{air}. Contour interval is 0.5°C. Contours −0.2° and 0.2°C are added. (c) As in (b), but for P. Contour interval is 0.2 mm day^{-1}. Contours −0.1 and 0.1 mm day^{-1} are added. (d)–(f) As in (a)–(c), but for the CPAC ENSO.

extratropics resembles a Pacific–North American (PNA) pattern. That supports an east–west contrast of the T_{air} pattern. Negative anomalies over the West Coast extend more inland to California. That is consistent with more rainfall over the Southwest. The weakening of negative anomalies over the Southeast indicates less rainfall there. The anomalies over the Ohio Valley depend on the location of positive anomalies over North America and are controlled by the convection in the tropics for a particular ENSO event. The jet stream shows the eastward extension to the west coast of North America.

5. Conclusions

Data from the observations and 20C3M model runs from the IPCC project were analyzed to study the decadal changes of the impact of ENSO over air temperature and precipitation over the United States. The observational study is limited by data availability. The model has biases. The combination of the data and model results allows us to reach the following conclusions:

As documented by Yeh et al. (2009), Ashok et al. (2007), and many others, there are two types of ENSO: EPAC

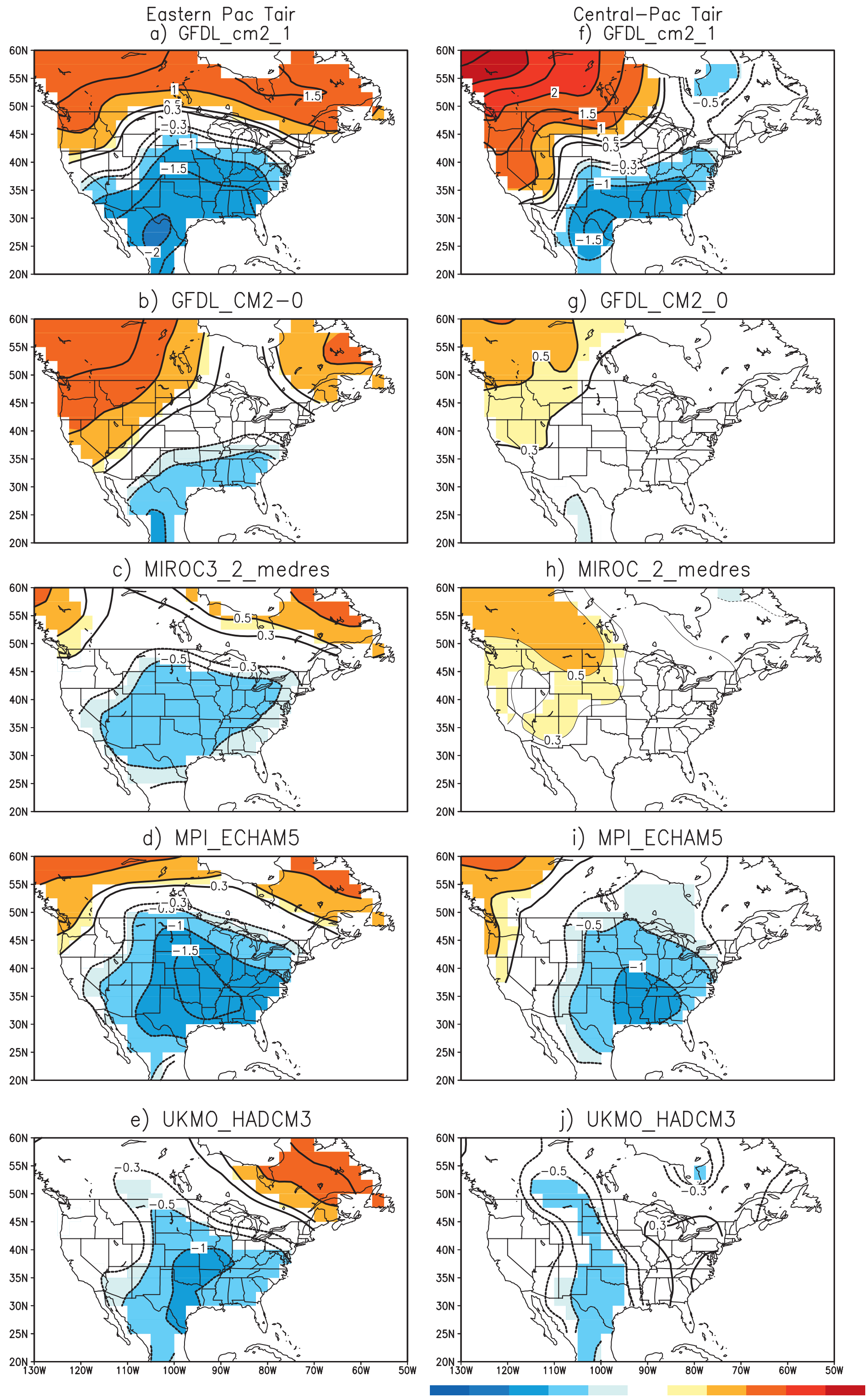

FIG. 9. As in Fig. 7, but for T_{air}. Contour interval is 0.5°C. Contours −0.3° and 0.3°C are added.

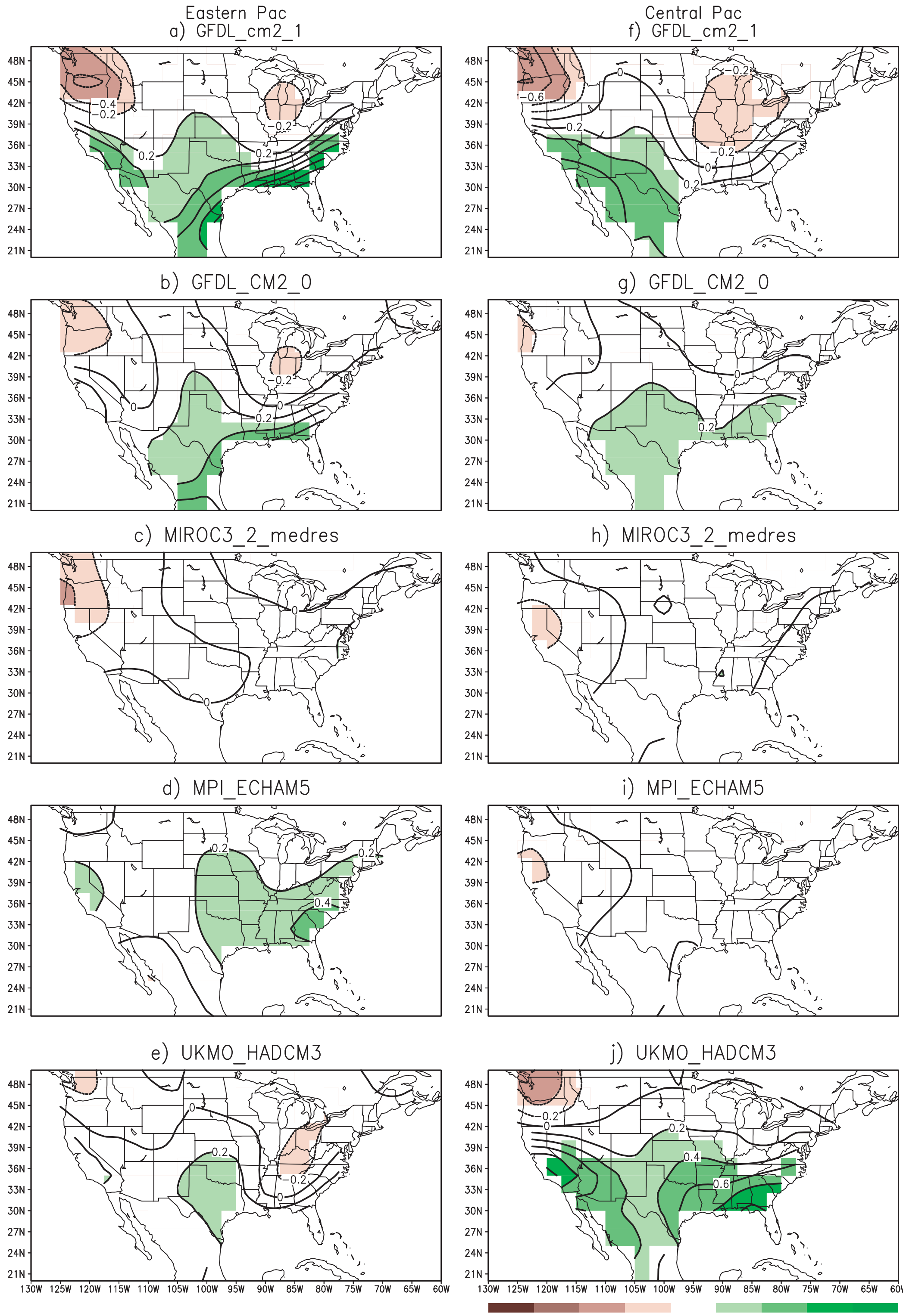

FIG. 10. As in Fig. 7, but for P anomalies. Contour interval is 0.2 mm day^{-1}.

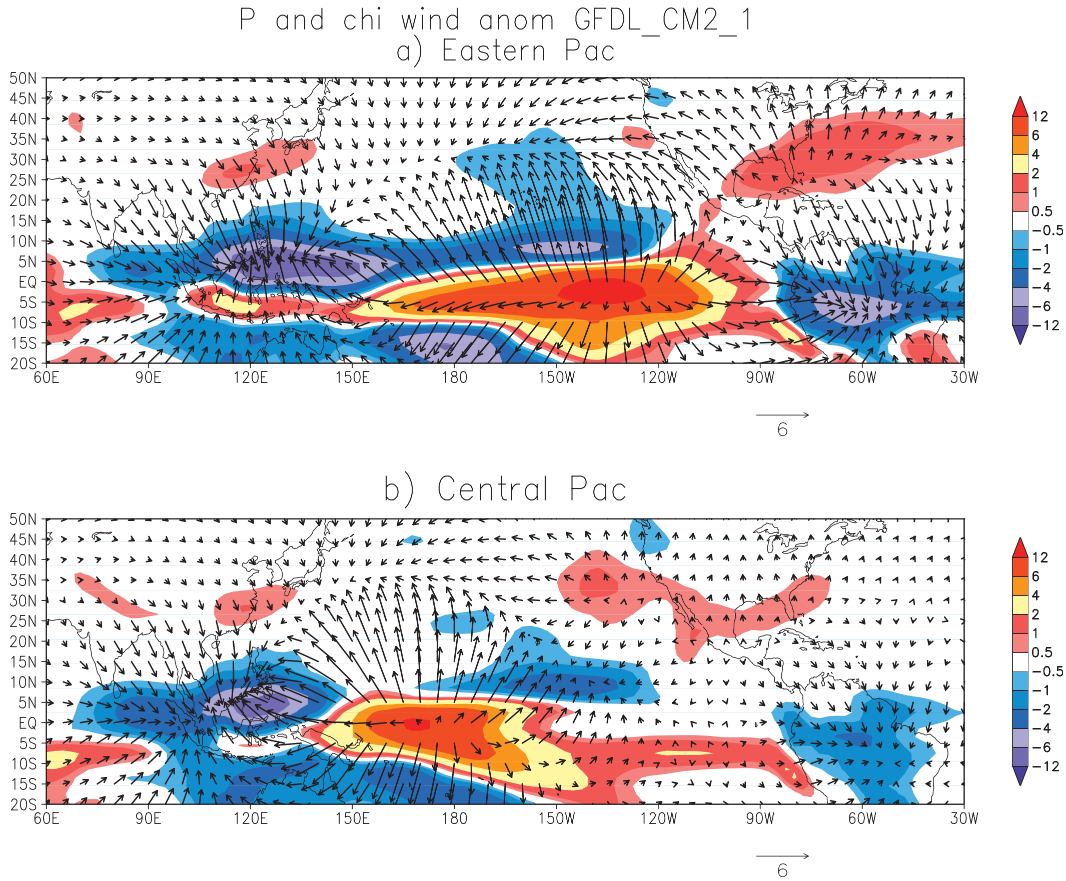

FIG. 11. (a) Composite of P anomalies from the GFDL CM2.1 for JFM (colored), and divergent Chi wind anomalies (vector) at 200 hPa for EPAC ENSO. The scale is 6 m s^{-1}. (b) As in (a), but for CPAC ENSO.

ENSO has the SSTA maximum over the eastern Pacific near 120°E and is the common kind; CPAC ENSO has an SSTA maximum in the central Pacific near the date line and started to appear after 1960. Yeh et al. (2009) suggested that there will be more CPAC events in a warmer climate.

The sensitivity experiments by Barsugli and Sardeshmukh (2002) suggested that the regional precipitation and circulation anomalies over the Pacific–North American region are sensitive to the exact locations of the SST anomalies in the tropical Pacific. For EPAC ENSO, enhanced convection extends from the date line to the eastern Pacific, with negative anomalies in the western Pacific. There is less rainfall over northern Brazil because of the Walker circulation. This creates a favorable condition for rain to occur over the Southeast. The atmospheric responses resemble a tropical Northern Hemisphere pattern with positive anomalies over the northern United States and Canada and negative anomalies to the south. The impact of the EPAC events on T_{air} is a north–south contrast pattern with cooling over the southern Plains and the Southeast, and warming to the north. There are large uncertainties of the location of the zero line, which separates warming from cooling. For P, there is less rainfall over the Pacific Northwest and the Ohio Valley and more rainfall over northern California and the Southeast.

The CPAC ENSO has convection centered at the date line, which is located westward of convection for the EPAC ENSO. The response shows a Pacific–North American pattern and supports the east–west contrast of the T_{air} pattern. Negative streamfunction anomalies extend more inland into the Southwest, which is consistent with the greater amount of rainfall there. Negative anomalies over the Southeast are weaker so there is less rainfall there. The largest uncertainties are the extent of warming over the west region and the P responses in the Ohio Valley. They may depend on the locations of anomalies of the PNA wave train.

The more frequent occurrence of the CPAC ENSO in the recent period may explain the decadal differences in the ENSO impact on the hydroclimate over the United States. The composites for the early period from 1915 to 1960 differ from composites for the recent period

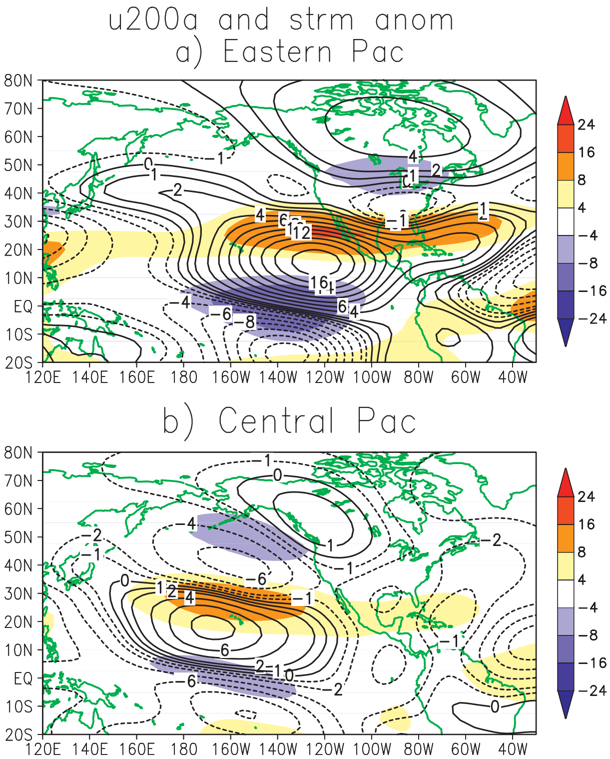

FIG. 12. (a) Composite of 200-hPa zonal *u* wind anomalies (colored) and streamfunction anomalies with zonal means removed (contoured) for EPAC ENSO. Contour interval is 2×10^6 m^2 s^{-1}. (b) As in (a), but for CPAC ENSO.

(1962–2006) in winter and spring. For temperature, the cooling over the south and warming over the north have been weakening for the recent period. For *P*, the ENSO influence over the Southwest was stronger over the recent period, while the impact over the Ohio Valley weakened. These differences are not due to long-term trends in T_{air} or *P*. They can be explained as the linear combination of the impacts of the CPAC and the EPAC ENSO events.

Seasonal forecasters often use composites of ENSO as one of the tools to examine the impact of ENSO over the United States. Composites based on early events may not be good indicators for the future climate. As suggested by Yeh et al. (2009), there will be more CPAC events in a warmer climate. How to construct composites becomes an important question needed to be addressed. Larkin and Harrison (2005a,b) also suggested that composites from all ENSO events may be misleading. Because the decadal differences of the ENSO impact can be explained by the weighted combination of the EPAC and CPAC events, the composites with "all" ENSO together are not representative. One needs to determine the type of ENSO for the current conditions. Then, composites for that type of ENSO may be used for projection.

Acknowledgments. The author wishes to thank Dr. Dennis Lettenmaier and his group from the University of Washington for providing *P* and T_{air} data from VIC. Thanks to Dr. Fiona Horsfall for encouragement. This work was supported by NCPO/CPPA Grant NA09OAR4310189.

REFERENCES

Andreadis, K. M., E. A. Clark, A. W. Wood, A. F. Hamlet, and D. P. Lettenmaier, 2005: Twentieth-century drought in the conterminous United States. *J. Hydrometeor.,* **6,** 985–1001.

Ashok, K., S. K. Beheria, S. A. Rao, H. Weng, and T. Yamagata, 2007: El Niño Modoki and its possible teleconnection. *J. Geophys. Res.,* **112,** C11007, doi:10.1029/2006JC003798.

Barsugli, J. J., and P. D. Sardeshmukh, 2002: Global atmospheric sensitivity to tropical SST anomalies throughout the Indo-Pacific basin. *J. Climate,* **15,** 3427–3442.

Bjerknes, J., 1966: A possible response of the atmosphere Hadley circulation to equatorial anomalies of ocean temperature. *Tellus,* **8,** 820–829.

Diaz, H. F., M. P. Hoerling, and J. K. Eischeid, 2001: ENSO variability, teleconnections and climate change. *Int. J. Climatol.,* **21,** 1845–1862.

Groisman, P. Ya., R. W. Knight, T. R. Karl, D. R. Easterling, B. Sun, and J. H. Lawrimore, 2004: Contemporary changes of the hydrological cycle over the continuous United States: Trends derived from in situ observations. *J. Hydrometeor.,* **5,** 64–85.

Hoerling, M. P., and A. Kumar, 2002: Atmospheric response patterns associated with tropical forcing. *J. Climate,* **15,** 2184–2203.

——, ——, and M. Zhong, 1997: El Niño, La Niña, and the nonlinarity of their teleconnections. *J. Climate,* **10,** 1769–1786.

Kao, H. Y., and J. Y. Yu, 2009: Contrasting eastern Pacific and central Pacific types of ENSO. *J. Climate,* **22,** 615–631.

Kug, J. S., F. F. Jin, and S. I. An, 2009: Two types of El Niño events: Cold tongue El Niño and warm pool El Niño. *J. Climate,* **22,** 1499–1515.

Kumar, K. K., B. Rajagopalan, and M. A. Cane, 1999: On the weakening relationship between the Indian monsoon and ENSO. *Science,* **284,** 2156–2159.

Larkin, N. K., and D. E. Harrison, 2005a: On the definition of El Niño and associated seasonal average U.S. weather anomalies. *Geophys. Res. Lett.,* **32,** L13705, doi:10.1029/2005GL022738.

——, and ——, 2005b: Global seasonal temperature and precipitation anomalies during El Niño autumn and winter. *Geophys. Res. Lett.,* **32,** L16705, doi:10.1029/2005GL022860.

McCabe, G. J., and M. D. Dettinger, 1999: Decadal variations in ENSO teleconnections with precipitation in the western United States. *Int. J. Climatol.,* **19,** 1399–1410.

Meehl, J. A., C. Covey, K. E. Taylor, T. Delworth, R. J. Stouffer, M. Latif, B. McAvaney, and J. F. B. Mitchell, 2007: The WCRP CMIP3 multimodel dataset: A new era in climate change research. *Bull. Amer. Meteor. Soc.,* **88,** 1383–1394.

Mo, K. C., and J. E. Schemm, 2008: Drought and persistent wet spells over the United States and Mexico. *J. Climate,* **21,** 980–994.

Rasmusson, E. M., and T. H. Carpenter, 1982: Variation in tropical sea surface temperature and surface wind fields associated with the Southern Oscillation/El Niño. *Mon. Wea. Rev.,* **110,** 354–384.

——, and K. C. Mo, 1993: Linkages between 200-mb tropical and extratropical circulation anomalies during the 1986–1989 ENSO cycle. *J. Climate,* **6,** 595–616.

Ropelewski, C. F., and M. S. Halpert, 1986: North American precipitation and temperature patterns associated with the El Niño/Southern Oscillation. *Mon. Wea. Rev.,* **114,** 2352–2362.

——, and ——, 1989: Precipitation patterns associated with the high index phase of the Southern Oscillation. *J. Climate,* **2,** 268–284.

Smith, T. M., R. W. Reynolds, R. E. Livezey, and D. C. Stokes, 1996: Reconstruction of historical sea surface temperatures using empirical orthogonal functions. *J. Climate,* **9,** 1403–1420.

Trenberth, K. E., and D. A. Paolino, 1980: The Northern Hemisphere sea-level pressure data set: Trends, errors and discontinuity. *Mon. Wea. Rev.,* **108,** 855–872.

Van Oldenborgh, G. J., and G. Burgers, 2005: Searching for decadal variations in ENSO precipitation teleconnection. *Geophy. Res. Lett.,* **32,** L15701, doi:10.1029/2005GL023110.

——, S. Philip, and M. Collins, 2005: El Niño in a changing climate: A multimodel study. *Ocean Sci.,* **1,** 81–95.

Wyrtki, K., 1975: El Niño the dynamic response of the equatorial Pacific Ocean to atmospheric forcing. *J. Phys. Oceanogr.,* **5,** 572–584.

Yeh, S. W., J. S. Kug, B. Dewitte, M. H. Kwon, B. P. Kirkman, and F. F. Jin, 2009: El Niño in a changing climate. *Nature,* **461,** 511–514, doi:10.1038/nature08316.